PERGAMON International Journal of Impact Engineering 26 (2001) 831–841

INTERNATIONAL JOURNAL OF IMPACT ENGINEERING

www.elsevier.com/locate/ijimpeng

THE RESPONSE OF LAYERED ALUMINUM NITRIDE TARGETS SUBJECTED TO HYPERVELOCITY IMPACT

KARL WEBER[1], TIMOTHY J. HOLMQUIST[2], and DOUGLAS W. TEMPLETON[3]

[1]Fraunhofer-Institut für Kurzzeitdynamik, Ernst-Mach-Institut, Eckerstrasse 4, D-79104 Freiburg i.Br., Germany; [2]Army High Performance Computing Research Center/NetworkCS, Minneapolis, MN 55415, USA; [3]U. S. Army Tank Automotive Research, Development, and Engineering Center, Warren, MI 48397, USA

Abstract— This work presents both experimental and computational ballistic results of layered Aluminum Nitride (AlN) targets. An L/D = 6 tungsten penetrator is used to impact AlN targets at a nominal impact velocity of 2100m/s. The primary objective of this work is to determine the ballistic performance of layered ceramic targets to hypervelocity impact. Various layering configurations are investigated including separating the AlN ceramic layers by thin, low impedance, polymethyl methacrylate (PMMA). PMMA thicknesses of 1 mm, 0.5 mm and 0 mm are used. The number of AlN ceramic layers is also investigated. Target configurations of two, four, six, and twelve layers are considered. All targets consist of 76.2 mm of AlN. The experiments show that target resistance decreases when PMMA is added. Target resistance is also reduced when more layers are used. A secondary objective of this work is to evaluate the ballistic effect of reducing the lateral dimension of the ceramic tile (reduction in self-confinement). The experiments show reduced target resistance when the lateral tile size is decreased. Computations of selected experiments are presented to provide insight into the behavior of the AlN targets. The computations capture the effect of layering, PMMA separation and lateral tile size and provide insight into the behavior of the ceramic when used in these types of configurations.

Keywords: aluminum nitride targets, hypervelocity impact, layer number, PMMA interlayer, lateral tile size, confinement, depth-of-penetration test, penetration depth, target resistance, time-resolved observation, Lagrangian hydrocode, JH-2 ceramic model, numerical simulation.

INTRODUCTION

The primary motivation for using ceramics in armor is the relatively high mass effectiveness that occurs due to ceramics low material density and high compressive strength. Ceramics in real applications need to be axially and laterally confined by steel, aluminum or fiber reinforced composites to achieve good protection efficiency.

The interest for ceramic materials as armor started in the United States and in the former Soviet Union in the 1950's and 1960's, respectively. Since that time a wide variety of ceramic materials such as glass, aluminum oxide (Al_2O_3), titanium diboride (TiB_2), silicone carbide (SiC), boron carbide (B_4C), and aluminum nitride (AlN) as well as fiber laminates have been investigated. Many of these ceramics have proven to be advantageous for terminal ballistic applications in light, medium and heavy armor systems against shaped charge jets as well as kinetic energy projectile threats.

Wilkins et al. (1969, 1971) tested thin ceramic plates with thin aluminum backing against short armor-piercing projectiles. Yaziv et al. (1986) introduced the differential and mass efficiency factors DEF and MEF, respectively, for ranking of ceramics using the Depth-of-Penetration (DOP) test. The DOP test was first proposed and carried out by Bless et al.

0734-743X/01/$ - see front matter
PII: S0734-743X(01)00136-1

(1987) and established by Woolsey et al. (1989, 1992), Mellgard et al. (1989) and Rosenberg and Tsaliah (1990). The DOP test is generally accepted in the community as a standard test methodology for ranking of ceramic armor.

Obtaining a time-resolved pseudo-cinematography of the interaction between projectile and ceramics can also be very helpful in understanding ceramic behavior. Hohler and Stilp (1984) used flash radiography to observe the penetration process of long rods into glass targets. Hauver et al. (1992) and Yaziv and Partom (1993) used the time-resolved observation technique, as well as the DOP test, for the examination of several ceramics. Hohler et al. (1995) and Reaugh et al. (1999) investigated the protection efficiency of numerous ceramics as a function of impact velocity. Orphal (1997) investigated phase three penetration into confined B_4C, AlN, and SiC ceramic targets in the velocity range 1.5 – 5 km/s.

El-Raheb (1993) has studied transient linear elastic wave propagation in finite periodic elastic media using one-dimensional analysis. El-Raheb and Wagner (1996) extended this one-dimensional theory to a two-dimensional consideration of axisymmetric finite layered periodic and weakly coupled stacks. They revealed that the occurrence of flexure in layered ceramic systems control attenuation and shape of the compressive wave along the stack. To investigate the effect of layering and confinement DOP tests with monolithic, two-, three- and six-layer aluminum nitride (AlN) ceramic targets bonded by thin polyurethane films were performed by Weber et al. (1999).

The primary goal of this work is to investigate the effect of separating AlN ceramic layers by thin PMMA films and to determine the influence of the number of AlN layers used in a given target of constant areal density. The work was motivated by the fact that thin ceramic layers are less expensive to manufacture than thick pieces, thus, if it could be demonstrated that performance is insensitive to layering, cost savings could be realized. Computations are also presented to provide insight into the behavior of the AlN targets.

EXPERIMENTAL SET-UP

The experiments were performed with tungsten sinter alloy rods with a blunt nose of D = 11 mm diameter, length-to-diameter ratio of L/D = 6 and mass of $m_P \approx 110$ g. The nominal impact velocity for all experiments was $v_P = 2100$ m/s. The projectile was accelerated by means of the EMI range 1 two-stage light gas gun with pump and launch tube diameters of 65 mm and 31 mm, respectively. A polycarbonate sabot with titanium inset for pushing of the rod was also used. After leaving the barrel the sabot parts are laterally deflected by aerodynamic forces and separated from the projectile (Fig. 1).

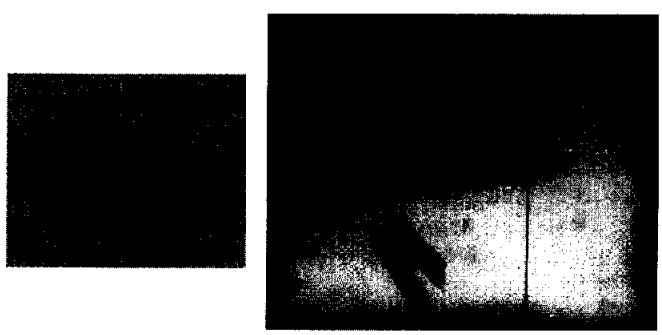

Fig. 1. In-flight separation of projectile and sabot by aerodynamic forces.

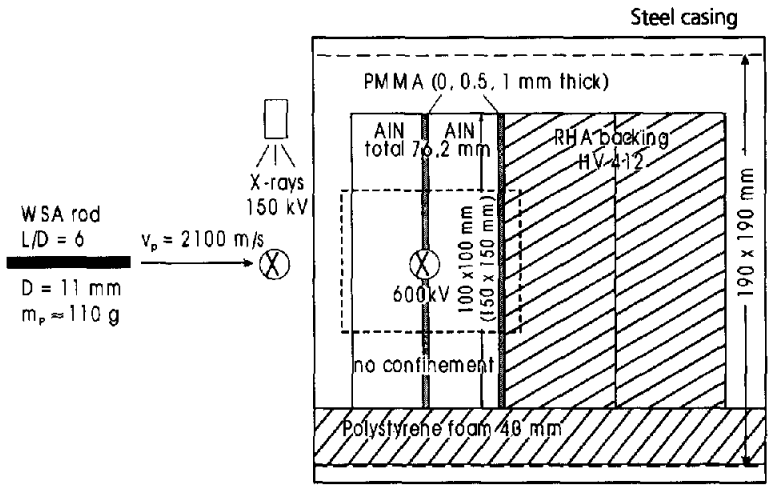

Fig. 2. Test set-up.

The test set-up used to determine the protection efficiency (residual penetration depth p_R) of the aluminum nitride (AlN) ceramic target is shown in Fig. 2. Two different test methods were applied: 1) the depth-of-penetration (DOP) test and 2) the time-resolved observation technique.

The ceramic targets tested in the DOP configuration consisted of two, three, four, six and twelve AlN tiles with layer thicknesses of 38.1 mm (1.5"), 25.4 mm (1"), 19.05 mm (0.75"), 12.7 mm (0.5") and 6.35 mm (0.25"), respectively. The total ceramic thickness of 76.2 mm (3") was constant for all targets and the lateral tile dimensions were 150 x 150 mm (6" x 6"). As backing material, two 50 mm thick RHA plates with a Vickers hardness number of HV20 = 412 were used.

The ceramic tiles were coupled by means of 0, 0.5 and 1 mm thick PMMA interlayers. All layers were bonded using a two-component epoxy resin adhesive with a controlled thickness of 0.1 mm to 0.23 mm. The same procedure was used to bond the ceramic stack to the RHA backing. For all experiments the ceramic tiles were laterally unconfined and no cover plate was used. Finally, in order to minimize shock wave transmission from the base plate into the ceramic stack, target and base plate (steel casing) were separated using a 40 mm thick piece of polystyrene foam. The 150 kV flash X-ray tubes, mounted both vertically and horizontally, allowed the determination of the projectiles' yaw and pitch angles, respectively, at the moment of projectile impact on the ceramic target.

In the second test set-up a 600 kV flash X-ray tube was applied for the time-resolved observation of the projectile–target interaction during penetration into the layered AlN ceramic stack. To obtain good contrast in the X-ray photographs the lateral AlN tile dimensions were reduced from 150 x 150 mm to 100 x 100 mm (4" x 4"). The influence of 0 mm and 1 mm thick PMMA films was investigated for two-layer (2 x 1.5") and twelve-layer (12 x 0.25") ceramic systems. In this set-up the target was encased but not confined by a steel tube of an inner cross section of 190 x 190 mm with a 140 x 50 mm wide observation window to avoid damaging of the technical equipment by ceramic fragments. The results of this target are also used to evaluate the effect of lateral tile dimension (self-confinement) on the target resistance.

MATERIAL PROPERTIES

The material properties of the tungsten projectile (WSA), AlN ceramic tiles and RHA backing are summarized in Table 1. The AlN ceramic tiles were produced by the DOW Chemical Company, Midland, MI, USA. The tiles consist of 95-100 % aluminum nitride, 0-5 % aluminum

oxide and 0-5 % yttrium oxide. The material density and boiling point of aluminum nitride is ρ = 3.26 g/cm^3 and T = 2423 K, respectively. The PMMA material density, longitudinal and shear wave velocities are ρ = 1.2 g/cm^3, C_L = 2760 m/s and C_S = 1380 m/s, respectively (Morris (1982)). An epoxy resin adhesive, WELDON-10 A&B, manufactured by the IPS Corporation, Gardena, CA, USA, was used to bond all materials.

Table 1. Material properties of WSA rod, AlN and RHA backing

Material	*Ultimate tensile strength (UTS) [MPa]*	*Hardness*	*ρ [g/cm^3]*	*A_5 [%]*
WSA	1550	----	17.6	7.1
RHA	1150	HV20=412	7.85	11

Material	*Grain size [μm]*	*Flexure strength [MPa]*	*Young's modulus [GPa]*	*Compression strength [GPa]*	*ρ [g/cm^3]*	*C_L [m/s]*
AlN (sintered)	3 – 10	235	310	3 – 4	3.26	10700

RESULTS AND DISCUSSION

Experimental Investigations

Table 2. Results of the depth-of-penetration tests

Exp. No.	*v_P [m/s]*	*α_1 / α_2 [deg]*	*Lateral tile dim. [mm]*	*No. of tiles*	*Total AlN tile thickness [mm]*	*Average AlN tile thickness [mm]*	*Average PMMA thickness [mm]*	*p_R p [mm]*	*MEF*	*DEF*
8401	2130	+1.5/---	150x150	12	76.3	6.36	1.0	27.9	1.52	1.98
8402	2132	+3.5/-1.0	150x150	12	76.3	6.35	0.5	25.4	1.59	2.06
8403	2133	+1.5/-0.5	150x150	12	76.2	6.35	0	23.5	1.64	2.12
8413	2129	+4.0/-1.0	150x150	6	76.6	12.8	1.0	20.1	1.74	2.21
8412	2134	+2.0/-0.5	150x150	6	76.8	12.8	0	19.8	1.75	2.22
8405	2120	+2.0/-0.5	150x150	4	77.2	19.3	1.0	22.2	1.67	2.15
8406	2128	+0.5/-0.5	150x150	4	76.4	19.1	0.5	21.6	1.70	2.17
8407	2120	0/-0.5	150x150	4	76.5	19.1	0	19.2	1.78	2.24
8411	2131	+2.0/-0.5	150x150	3	76.3	25.4	1.0	23.8	1.63	2.11
8408	2129	+2.0/-0.5	150x150	2	76.2	38.1	1.0	26.7	1.55	2.02
8409	2124	+3.0/-0.5	150x150	2	76.2	38.1	0.5	20.6	1.73	2.21
8410	2118	+2.5/-1.0	150x150	2	76.1	38.1	0	16.0	1.90	2.36
8399	1975	+1.5/---	150x150	---	3x50 RHA	---	---	89.8	---	---
8400	1996	+2.5/-0.5	150x150	---	3x50 RHA	---	---	91.4	---	---
8414	2120	-0.5/-0.5	150x150	---	3x50 RHA	---	---	90.4	---	---
8418	2108	+1.0/0	100x100	12	75.8	6.32	1.0	31.1	1.45	1.89
8417	2123	+1.0/-0.5	100x100	12	76.2	6.35	0	28.6	1.50	1.96
8416	2119	+1.0/-0.5	100x100	2	76.2	38.1	1.0	25.7	1.58	2.05
8415	2116	+0.5/-0.5	100x100	2	76.4	38.2	0	26.4	1.56	2.02

Table 2 summarizes the results of the depth-of-penetration (Exps. 8401 through 8413) and time-resolved observation tests (Exps. 8415 through 8418) against AlN tiles with lateral dimensions of 150 x 150 mm and 100 x 100 mm, respectively. The residual penetration depth p_R (measured into the RHA backing), as well as the corresponding mass and differential efficiency factors (MEF and DEF), the number of AlN layers and the PMMA interlayer thickness are all listed for each test.

The values of MEF and DEF are calculated according to the definition given by Hohler et al. (1995) by means of the residual penetration depth p_R and penetration depth p (Exps. 8399, 8400 and 8414) measured in semi-infinite RHA.

The test results show that increasing the number of AlN layers increases the residual penetration depth p_R. Bonding the AlN layers with PMMA interlayers also results in increasing p_R. p_R continues to increase with increasing PMMA sheet thickness. The lowest p_R values were found for ceramic stacks without PMMA, bonded with two-component epoxy resin adhesive. The highest p_R was measured in the case of the 1 mm PMMA films. The reason for this behavior is reduction of the stiffness of the ceramic stack by including the weak PMMA interlayers as demonstrated by numerical simulations discussed later.

Reduction of the lateral tile dimensions from 150 x 150 mm to 100 x 100 mm also leads to higher p_R values due to the decrease of self-confinement.

In case of the 150 x 150 mm ceramic tiles MEF and DEF range between 1.6 – 1.9 and 2.0 – 2.35, respectively. The mass and differential efficiency factors are diminished to MEF = 1.45 – 1.6 and DEF = 1.9 – 2 for the 100 x 100 mm AlN ceramics.

To investigate the PMMA layer influence on the projectile–ceramic target interaction process, experiments were performed against two- and twelve-layer AlN ceramic stacks varying the PMMA interlayer thickness in between the ceramic tiles from 0 to 1 mm. The test results are summarized in Table 3, and the corresponding parameter definitions are given in Fig. 3.

Table 3. Results of the time-resolved observation tests

Exp. No.	v_P *[m/s]*	t *[μs]*	s_K *[mm]*	s_H *[mm]*	l *[mm]*	u *[m/s]*	v *[m/s]*	u/v_P	v/v_P	*No. of AlN tiles*	*Average AlN tile thickness [mm]*	*Average PMMA thickness [mm]*
8415	2116	~21	27.0	43.4	49.6	1290	2070	0.61	0.98	2	38.2	0
8416	2119	47.2	56.7	92.7	30.0	1201	2025	0.57	0.96	2	38.1	1.0
8417	2123	47.3	58.5	93.2	31.3	1237	2027	0.58	0.96	12	6.35	0
8418	2108	40.1	55.1	81.0	40.1	1374	2039	0.65	0.97	12	6.32	1.0

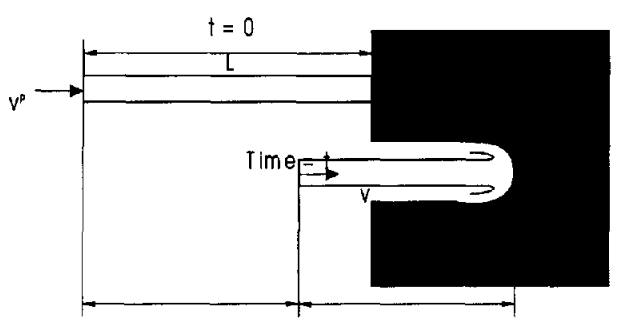

Fig. 3. Definition of parameters of time-resolved observation tests.

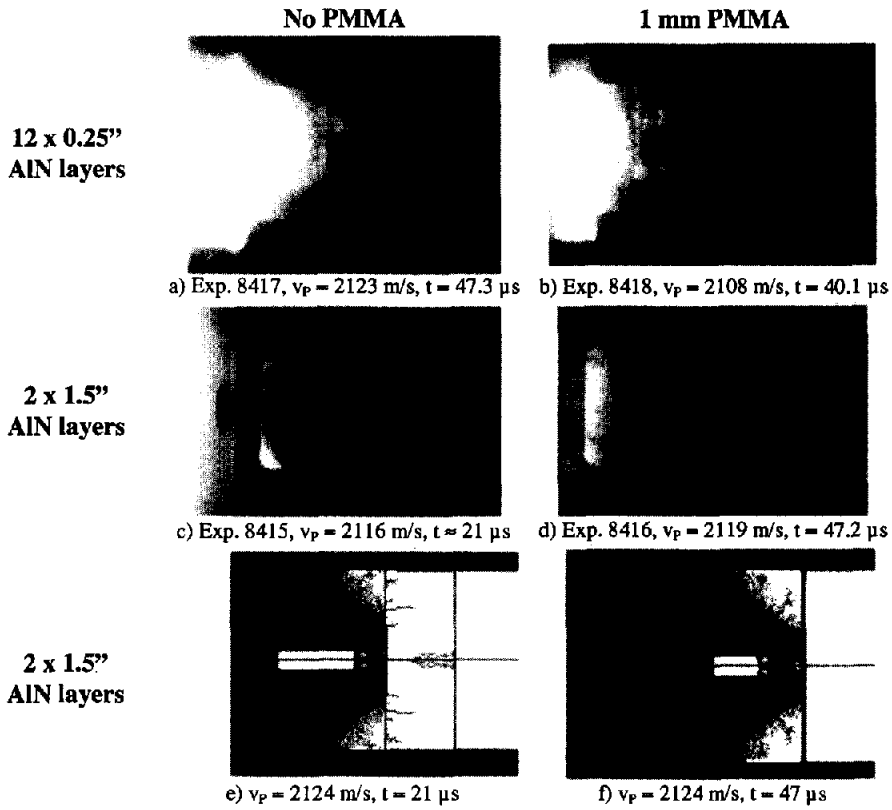

Fig. 4. PMMA-layer influence on the projectile – target interaction during penetration of a L/D = 6 WSA rod into two- and twelve-layer AlN ceramic targets. Comparison between experiments and numerical simulation.

The 600 kV flash X-ray photographs of the time-resolved observation tests are shown in Fig. 4. For the twelve-layer target (Figs. 4a and 4b) the flash X-rays are taken at comparable times (47 μs and 40 μs after impact). It can be seen that including the 1 mm PMMA films in between the tiles causes a larger lateral spread of the eroded penetrator material resulting in a larger momentary crater diameter.

Figs. 4c and 4d present the X-ray photographs for the two-layer targets. Because of a trigger malfunction, the photograph of Exp. 8415 is taken earlier (t ≈ 21 μs) than in Exp. 8416 (t = 47.2 μs), but still provides useful information. In Fig. 4c (no PMMA) the penetrator has not yet reached the epoxy resin bond and the crater appears to be still relatively narrow. In Fig. 4d the rod has already passed the 1 mm PMMA interlayer resulting in a larger crater diameter caused by the stronger WSA spread.

Comparison of Figs. 4b and 4d show that the lateral WSA spread at the PMMA interlayer seems to be larger for the two- than for the twelve-layer target. This may be due to the mitigation of ceramic fracture at the PMMA-ceramic interface.

The numerical simulations carried out for the two-layer stack, without PMMA (Fig. 4e) and with 1 mm PMMA (Fig. 4f), underestimate the crater channel diameter observed in the experiments, although the penetration depths seem to be reasonable. This crater diameter may be better represented by the area of failed ceramic material (failed ceramic represented by the shaded region). Also note how the fractured ceramic is arrested at the interface in Fig 4e. More indepth discussions of the computations are presented in the following section.

Numerical Simulation

This section presents computations of selected layered ceramic target configurations presented in Table 2. The objective of the computations is to provide insight into the effect of layering, PMMA interlayer thickness, and lateral tile dimension. All the computations were performed using a Lagrangian hydrocode (Johnson et al. 1997) in axisymmetric geometry. Five crossed triangles across the penetrator radius, with an aspect ratio of one, was the zoning pattern used.

Recently, computations of DOP experiments of layered AlN ceramic targets were performed and produced results that are in good agreement with test data (Holmquist et al. (2000)). The work presented herein uses the same JH-2 ceramic model (Johnson and Holmquist (1994)) and the same AlN material model constants as used previously (Holmquist et al. (2000)). This work differs from previous work in that all impacts are hypervelocity, and the effect of PMMA and lateral tile size is investigated.

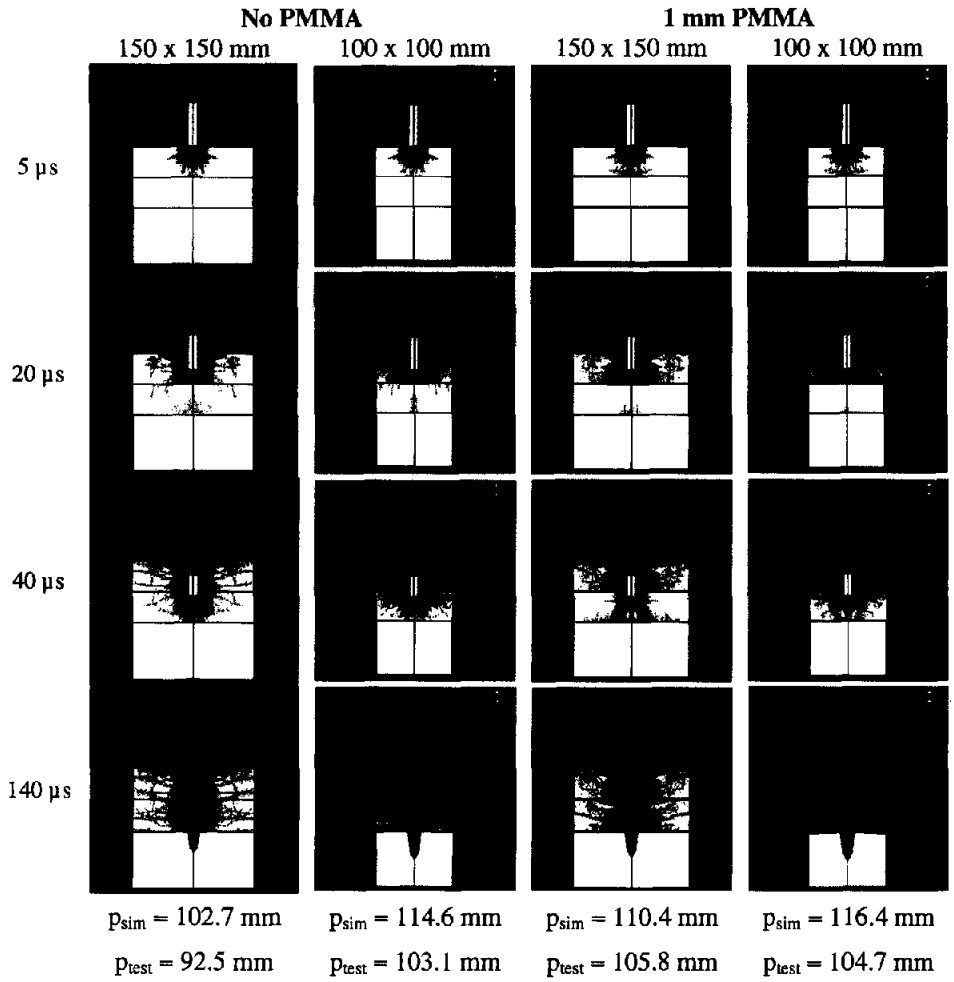

Fig. 5. Comparison of the computational results for 150 mm x 150 mm and 100 mm x 100 mm AlN ceramic tiles with 0 mm and 1 mm PMMA interlayers at $v_P = 2100$ m/s.

Four target configurations with lateral dimensions of 100 mm x 100 mm and 150 mm x 150 mm were considered: 1) Two-layer AlN target without PMMA, 2) Two-layer AlN target with 1 mm PMMA, 3) Six-layer AlN target without PMMA, 4) Six-layer AlN target with 1 mm PMMA. The computations also included the thin film of epoxy resin adhesive (~0.2 mm thick) used to bond the tiles and PMMA when required.

Figures 5-8 present the results of the computations. Figure 5 presents computational results for the 150 mm x 150 mm and the 100 mm x 100 mm target with a 0 mm and a 1 mm PMMA interlayer. The results are presented at 5 μs, 20 μs, 40 μs and 140 μs after penetrator impact. All the computations are complete at 140 μs. The shaded regions indicate material that is completely fractured. The final penetration results for the simulations, p_{sim}, and the test, p_{test}, are listed at the bottom of Fig. 5 and presented in bar graph form in Fig. 7. The computational results overpredict the experiments by approximately 10%, but appear to capture the trends. Both the computations and experiments indicate a reduction in target performance when lateral tile size is reduced and when a PMMA layer is added. The computational results provide some explanation for this behavior. When the PMMA is added the relatively soft material reduces the rear support of the AlN, and the shear coupling between ceramic layers. This causes the AlN to fracture (damage) more easily at the ceramic/PMMA interface as shown at 5 μs and 20 μs in Fig. 5. Ceramic performance is known to be sensitive to rear surface support and tensile failure and the results herein are consistent with previous work (Wilkins et al. (1969, 1971)).

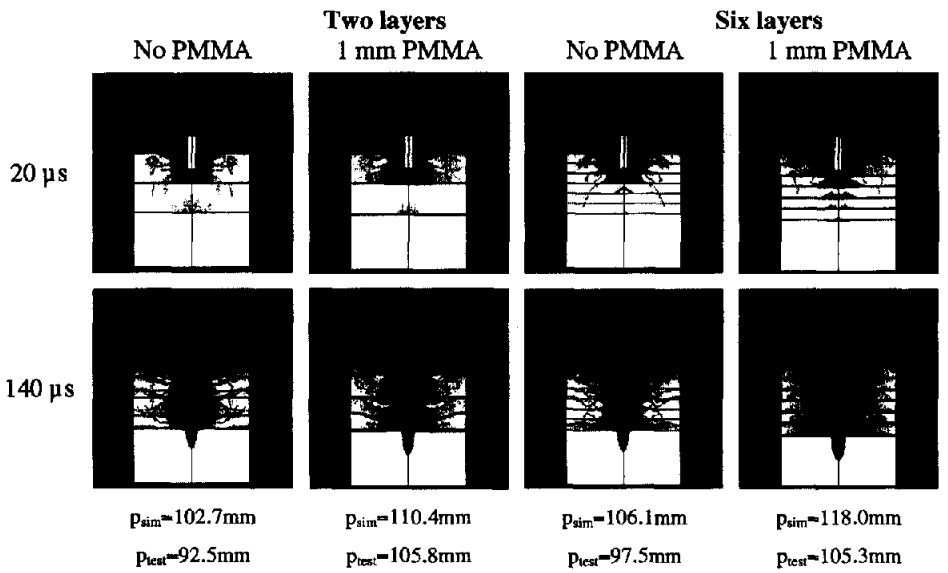

Fig. 6. Influence of layering and PMMA interlayer on damage behavior and protection efficiency for the 150 mm x 150 mm AlN ceramic target.

Tile size effect is also presented in Fig. 5. The computations show increased penetration when the tile size is reduced. When the tile size is reduced there is less lateral material to maintain the confinement pressure. Reduced pressure results in a lower material strength and thus increased penetration. This is most apparent at 140 μs where the 100 mm x 100 mm targets have clearly expanded in the radial direction indicating reduced confining pressure.

Figures 6-8 present the effect of layering, with and without the PMMA interlayer. Figure 6 presents the computed results at 20 μs and 140 μs after penetrator impact for the two- and six- layer target. The computations are complete at 140 μs and again the shaded region indicates completely fractured material. Careful examination of the computations identifies why layering

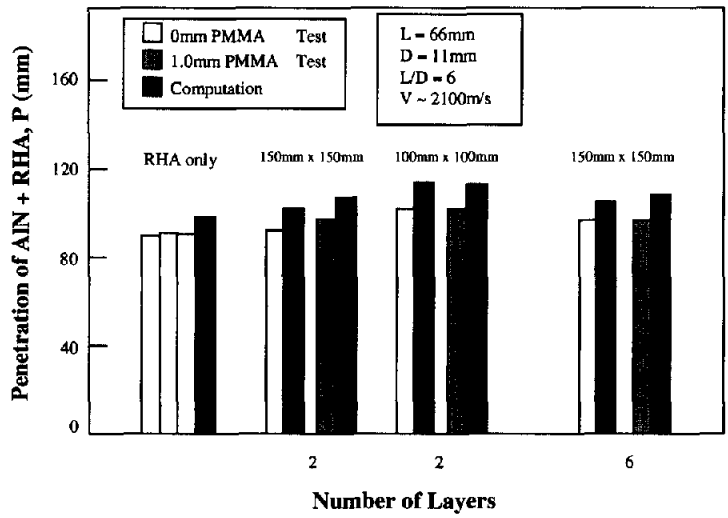

Fig. 7. Experimental and computational total penetration depth in two- and six-layer targets, for the 150 mm x 150 mm and 100 mm x 100 mm AlN stacks with 0 mm and 1 mm PMMA.

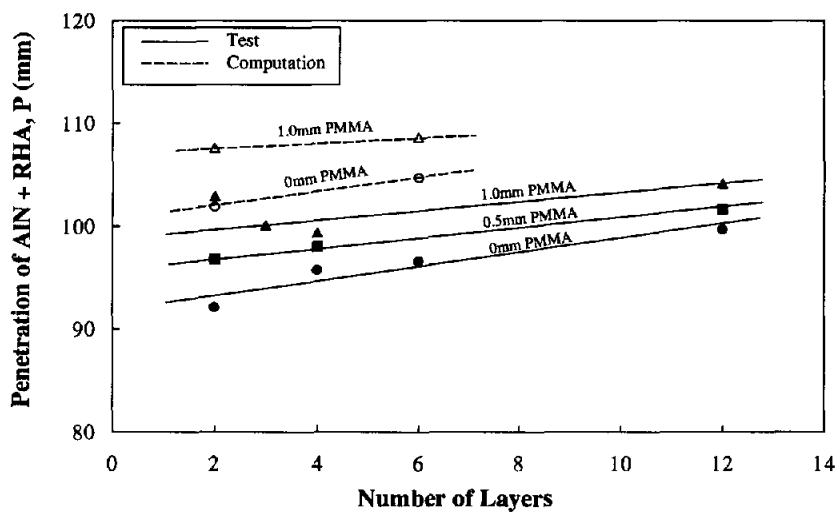

Fig. 8. Total penetration depth versus number of AlN layers determined by experiments and numerical simulations for the 150 mm x 150 mm targets.

reduces target ballistic performance. The computations show that in the six layer target the damage initiates at the rear surface of the individual tiles and propagates upward through the tile. The damage that occurs by this process is dominated by tensile failure. Because ceramic is weaker in tension than compression it takes less energy to fail ceramic in tension. The six-layer target is dominated by tensile failure and thus exhibits a softer response. Including PMMA films in between the tiles simply enhances this effect by reducing the shear coupling between layers. In contrast, the two-layer target is much stiffer resulting in more of the ceramic failing in compression. The final penetration depths, for both the simulation and test, are presented at the

bottom of Fig. 6 and compared graphically in Figs. 7 and 8. The computations overpredict the test results by approximately 10 % but again appear to capture the correct trends. Another interesting observation is the apparent increase in damaged material in the targets that include the PMMA. This is consistent for both the two layer and six layer targets. The radiographs in Fig. 4 (Exps. 8415, 8416) tend to show this same behavior.

CONCLUSIONS

In this experimental and computational study, the ballistic effect of separating AlN ceramic layers by thin low impedance PMMA, layering of the ceramic, and lateral ceramic tile size was investigated for hypervelocity impact. The results indicate reduced target resistance when PMMA is added caused by reduced shear coupling between the ceramic layers and reduced rear surface support. Layering of the ceramic also reduced target resistance, because the target becomes less stiff and more susceptible to bending and tensile failure. These effects increase as the PMMA thickness increases, although the influence of the PMMA has a smaller effect when many layers are used. This is probably because the system is already overly soft. Target resistance is also reduced when the lateral tile size is decreased. This occurs due to a reduction in the lateral confinement resulting in reduced ceramic strength. Computations of the experiments were also presented and provided insight into the behavior of the AlN targets. The computations captured the effect of PMMA separation, layering and lateral confinement.

Acknowledgement—We would like to gratefully thank Dr. Michael El-Raheb, Midland, MI, USA, for his appreciated advice during this study. This work was sponsored in part by the US Army, Army Research Laboratory, Army HPC Research Center. No official endorsement should be inferred.

REFERENCES

[1] Bless SJ, Rosenberg Z, Yoon B. Hypervelocity penetration of ceramics. *Int. J. Impact Engng*, 1987; **5**, 165-171.

[2] El-Raheb M. Transient elastic waves in finite layered media: One-dimensional analysis. *J. Acoust. Soc. Am.*, 1993; **94**(1).

[3] El-Raheb M, Wagner P. Transient elastic waves in finite layered media: Two-dimensional axisymmetric analysis. *J. Acoust. Soc. Am.*, 1996; **99**(6).

[4] Hauver GE, Netherwood PH, Benck RF, Gooch WA, Perciballi WJ, Burkins WS. Variation of target resistance during long rod penetration into ceramics. *Proc. 13th Int. Symp. Ballistics*, Stockholm, Sweden, 1992.

[5] Hohler V, Stilp AJ. Visualization of the penetration process of rods into glass and armor steel targets by means of flash X-ray photographs. *Proc. 35th ARA Meeting*, Meppen, Germany, 1984.

[6] Hohler V, Stilp AJ, Weber K. Hypervelocity penetration of tungsten sinter alloy rods into alumina. *Proc. of the 1994 Hypervelocity Impact Symposium*, Santa Fe, NM, USA, 1995; **17**, 409-418.

[7] Holmquist TJ, Templeton DW, Bishnoi KD. Constitutive modeling of aluminum nitride for large strain, high strain rate, and high pressure applications. Submitted to *Int. J. Impact Engng*, Received May, 2000.

[8] Johnson GR, Holmquist TJ. An Improved Computational Constitutive Model for Brittle Materials, *High Pressure Scie. and Tech.-1993*, AIP Press, NY, 1994.

[9] Johnson GR, Stryk RA, Holmquist TJ, Beissel SR. Numerical Algorithms in a Lagrangian Hydrocode. Report No. WL-TR-1997-7039, Wright Laboratory, June, 1997.

[10] Mellgard I, Holmberg L, Olsson LG. An experimental method to compare the ballistic efficiencies of different ceramics against long rod projectiles. *Proc. 11th Int. Symp. Ballistics*, Brussels, Belgium, 1989.

[11] Morris CE. Los Alamos shock wave profile data. *University of California Press*, Berkeley and Los Angeles, CA, 1982.

[12] Orphal DL. Phase three penetration. *Int. J. Impact Engng*, 1997; **20**, 601-616.

[13] Reaugh JE, Holt AC, Wilkins ML, Cunningham BJ, Hord BL, Kusubov AS. Impact studies of five ceramic materials and pyrex. *Int. J. Impact Engng*, 1999; **23**, 771-782.

[14] Rosenberg Z, Tsaliah J. Applying Tate's model for the interaction of long rod projectiles with ceramic targets. *Int. J. Impact Engng*, 1990; **9**(2), 247-251.

[15] Weber K, El-Raheb M, Hohler V. Experimental investigations on the ballistic performance of layered AlN ceramic stacks. *Proc. 18th Int. Symp. Ballistics*, San Antonio, TX, 1999.

[16] Wilkins ML, Cline CF, Honodel CA. Fourth progress report of light armor program. *Lawrence Radiation Lab. Rept.* UCRL-50694, 1969.
[17] Wilkins ML, Landingham RL, Honodel CA. Fifth progress report of light armor program. *Lawrence Radiation Lab. Rept.* UCRL-50980, 1971.
[18] Woolsey P, Mariano S, Kokidko D. Alternative test methodology for ballistic performance ranking of armor ceramics. *Proc. 5th Annual TACOM Armor Coordinating Conference,* Monterey, CA, ÚSA, 1989.
[19] Woolsey P. Ceramic materials screening by residual penetration ballistic testing. *Proc. 13th Int. Symp. Ballistics,* Stockholm, Sweden, 1992.
[20] Yaziv D, Partom Y. The ballistic efficiency of thick alumina targets against long rod penetrators. *Proc. 14th Int. Symp. Ballistics,* Québec City, Canada, 1993.
[21] Yaziv D, Rosenberg G, Partom Y. Differential ballistic efficiency of appliqué armor. *Proc. 9th Int. Symp. Ballistics,* Shrivenham, UK, 1986.